Effect of precursor and composition on the physical properties of the low-cost solution processed Cu_2ZnSnS_4 thin film for solar photovoltaic application

Goutam Kumar Gupta and Ambesh Dixit

Citation: J. Renewable Sustainable Energy **9**, 013502 (2017); doi: 10.1063/1.4974341
View online: http://dx.doi.org/10.1063/1.4974341
View Table of Contents: http://aip.scitation.org/toc/rse/9/1
Published by the American Institute of Physics

Effect of precursor and composition on the physical properties of the low-cost solution processed Cu_2ZnSnS_4 thin film for solar photovoltaic application

Goutam Kumar Gupta and Ambesh Dixit[a)]
Department of Physics and Center for Solar Energy, Indian Institute of Technology Jodhpur, Rajasthan 342011, India

(Received 22 September 2016; accepted 6 January 2017; published online 24 January 2017)

Quaternary compound semiconductor Cu_2ZnSnS_4 (CZTS) has been prepared using two different precursors sols, chlorides and nitrates, using spin coating process to get phase pure and less defective thin films for solar photovoltaics. The synthesized CZTS thin films are heat treated at different temperatures to achieve the kesterite crystallographic phase. The prepared thin films are highly textured along (112) axis. The surface microscopic images suggest that chloride precursor derived CZTS thin films are relatively uniform and densely packed as compared to nitrate precursors. The dislocation density is $\sim 1 \times 10^{16}$ lines m^{-2} for the chloride precursor derived thin films, much lower than that of the nitride precursor derived CZTS thin films. The optical absorption measurements suggest the direct optical gap ~ 1.52 eV for CZTS thin films derived from both the precursor routes. However, electrical resistivity measurements suggest that resistivity is uniform and much lower ~ 0.025 Ω cm for chloride precursor CZTS thin films, alike nitride precursor CZTS thin films, where resistivity is three orders of magnitude higher $\sim 30\,\Omega$ cm. These studies suggest that chloride precursor derived CZTS thin films are of high quality and can be used for solar photovoltaic applications. *Published by AIP Publishing.* [http://dx.doi.org/10.1063/1.4974341]

I. INTRODUCTION

Quaternary compound semiconductor $Cu_2ZnSnS_4(Se_4)$ (CZT(S,Se)) is drawing considerable attention as an absorber layer material for heterostructure thin film solar cells. The easy availability of material, low cost, non-toxicity, and the optimum direct bandgap ~ 1.5 eV makes Cu_2ZnSnS_4 (CZTS)(Se) suitable for replacing its counterpart $Cu(In,Ga)Se_2$(CIGS) compound semiconductor-based solar photovoltaic (PV) absorber. The laboratory cell efficiency beyond 20% has already been reported for the most efficient technologies, e.g., $Cu(In,Ga)Se_2$ (CIGS) and CdTe base solar cells and currently being explored for large area solar photovoltaic applications.[1,2] However, the toxicity of Cd and Ga and the scarcity of In and Te pose the economic and environmental sustainability challenges for these technologies. The near optimum bandgap of kesterite CZTS and its high absorption coefficient $>10^4\,cm^{-1}$ make it suitable for thin film absorber based photovoltaic devices and has the potential to replace the existing PV technologies. CZTS compound semiconductor is found in kesterite, stannite, and wurtzite crystallographic structures. Among them, the kesterite phase is thermodynamically more stable and thus can be synthesized in bulk or thin film geometries. However, the low thermal stability under typical synthesis condition and vulnerability to form impurity phases of binary sulfides and metal complexes put challenges in phase pure synthesis of the CZTS material.

This pure sulfide-based kesterite CZTS is an attractive semiconductor as it does not contain toxic elements such as Ga and Cd. However, the reported efficiency of pristine kesterite CZTS

[a)]Author to whom correspondence should be addressed. Electronic mail: ambesh@iitj.ac.in

is relatively lower, which can be enhanced by using sulfoselenide based kesterite and, $CZT(S,Se)_4$ absorber systems. However, near optimum bandgap of pure sulfide kesterite suggests enhanced performance than sulfoselenide kesterite theoretically. In conjunction with solar photovoltaic applications, CZTS has shown promise for numerous other applications such as a counter electrode for dye-sensitized solar cell (DSSC),[3,4] gas sensor,[5,6] and photocatalyst for hydrogen production.[7–9]

A typical CZTS planar solar cell structure configuration is shown schematically in Fig. 1. This is a multilayered Ni-Al-Grid/Al:ZnO/i-ZnO/CdS/CZTS/Molybdenum (Mo)/Sodalime glass (SLG) substrate based heterostructure solar photovoltaic device. The sodalime glass, as a substrate, assists sodium diffusion through molybdenum, which helps in larger grain growth of the CZTS absorber material.[10,11] Molybdenum on the SLG substrate acts as a metallic back reflector because of its low resistivity and assists in molybdenum disulfide (MoS_2) layer formation, which is useful for ohmic contact with the CZTS layer. MoS_2 also helps in absorption of the incident solar irradiance due to its lower indirect optical gap ($\sim$1.3 eV).[12] However, MoS_2 layer also prevents Na to diffuse into the CZTS absorber layer, hence precise control in the formation of MoS_2 is necessary.[12] The cadmium sulfide (CdS) layer acts as an n-type buffer layer and intrinsic i-ZnO as a window layer. Several alternatives to CdS such as ZnS, In_2S_3, etc., are also under investigation for solar photovoltaic applications. The conducting aluminum-doped zinc oxide (Al:ZnO) acts as the front contact material, where Ni:Al grids can be structured as electrical-connects for extracting the photo-generated electrons.

This configuration of solar cell has shown high efficiencies with CZTS in different geometrical structures. The nano-porous CZTS with the three-dimensional (3D) integration of CdS in thin film solar cell configuration has shown $\sim$5.02% photovoltaic efficiency.[13] The CZTS has also been employed in Dye-Sensitized Solar Cell (DSSC) structure and good photoresponse has been observed.[14] These applications rely on the phase pure synthesis of CZTS compound semiconductor, especially in the kesterite crystallographic phase. In recent years, several approaches both vacuum such as RF magnetron sputtering,[15] reactive sputtering,[16,17] thermal evaporation,[18] and non-vacuum such as spin coating,[19–23] spray pyrolysis,[24] successive ion layer adsorption reaction (SILAR),[25,26] solvothermal,[27] etc., have been investigated and developed for the growth of CZTS material either in bulk or nano-crystal geometries. The non-stoichiometric compositions, in particular, Cu-poor and Zn-rich CZTS material, have shown enhanced efficiency. However, the non-stoichiometry in CZTS is very prone to the growth of secondary phases, such as binary and ternary metal sulfides and crystal defects, hampering the solar photovoltaic performance. The present work focuses on the development of kesterite phase CZTS materials in thin film geometries using low-cost solution based spin coating process using

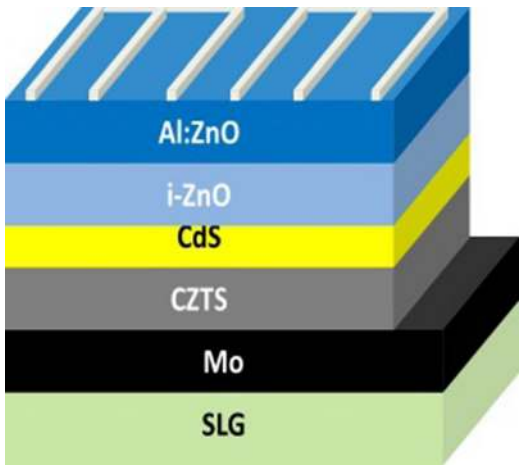

FIG. 1. The schematic multilayer stacking for heterostructure CZTS thin film solar cell structure, including soda lime glass (SLG) as a substrate, molybdenum as back contact layer, CZTS as an absorber layer, CdS as a buffer layer, intrinsic ZnO as a window layer, and Al-doped ZnO as a top electrode with Ni:Al grids for photoelectron collection.

different precursors and their impact on morphological, optical, and electronic properties, which may be useful for solar photovoltaic applications.

II. EXPERIMENTAL DETAILS

A. Synthesis

The chloride precursor solution was prepared using Cu, Zn, and Sn metal chlorides in the desired 2:1:1:8 compositional ratios. The 0.04 M Copper (II) chloride dihydrate ($CuCl_2{\cdot}2H_2O$, $\geq$99% Alfa Aesar), 0.02 M anhydrous zinc chloride ($ZnCl_2$, $\geq$98% Alfa Aesar), and 0.02 M Tin(II) chloride ($SnCl_2{\cdot}2H_2O$, $\geq$98%, Sigma Aldrich) are taken as metal sources, and thiourea is used to provide sulfur in the solution. These metal salts are dissolved successively in 2-methoxy ethanol (2-metho) ($\geq$99% Sigma-Aldrich) with 50 ppm butylhydroxytoluene (BHT) as a stabilizer, under continuous magnetic stirring. After dissolving metal salts, 0.16 M thiourea ($(NH_2)_2CS$, $\geq$99% Himedia) has been slowly introduced into the reaction mixture to initiate the reaction under continuous stirring for 1 h. The initial dark green color copper chloride solution turned into the light green color after adding zinc chloride precursor, which further turned into colorless transparent solution after adding the tin chloride. Finally, after adding thiourea, CZTS sol formation started with metal and thiourea complexes and turned into a yellow colored transparent sol after completing the process. The final solution, thus, prepared contains metal ions and thiourea complex. When thiourea was used in the stoichiometric ratio in the chloride precursor assisted route, the solution became a thick paste and the resulted sol was not suitable for spin coating. In this work, two times thiourea is used to form the desired molar ratio of sulfur for preparing a highly stable CZTS sol. The excess of thiourea has been considered during synthesis, avoids the sulfur loss during post-synthesis annealing of the pristine spin coated samples, and even more importantly, the preparation of stable sol for these metal precursors, essential for the spin coating process. The probable chemical reactions for CZTS sols are summarized in Table I. Several attempts were tried making a stable sol using methanol and ethanol with deionized (DI) water as a solvent but the prepared solution was not stable and the solution was precipitating in a day or two. After using 2-methoxy ethanol, a polar solvent has resulted into a highly stable (over several months period), yellow colored sol, which was further used for preparing thin films using spin-coating process.

In addition to the chloride precursors, we also attempted to make a highly stable sol using nitrate precursors for the growth of CZTS thin films. Here, metal nitrates such as copper(II) nitrate hemi-pentahydrate ($CuN_2O_6{\cdot}5H_2O$), Zinc nitrate hexahydrate($N_2O_6Zn{\cdot}6H_2O$), stannous chloride ($SnCl_2{\cdot}2H_2O$), and Thiourea (CH_4N_2S) precursors were used in the desired molar ratio of Cu:Zn:Sn:S::2:1:1:4 for synthesis of a stable CZTS sol. Here, in nitrate precursors route, the desired molar ratio of thiourea was sufficient to synthesize a stable sol. The probable chemical processes are summarized in Table I. Any attempt with excess thiourea has resulted in a stable sol solution; however, the thin films with excess thiourea with nitrate precursors have shown poor adherence to the substrate surface. Thus, any precursor with nitrate metal complexes and excess thiourea has degraded the film quality and has not been used further for any studies. The

TABLE I. Probable reaction path for the CZTS formation in chloride and nitrate precursor routes.

Proposed reaction in chloride route	Proposed reaction in nitrate route
$Cu(Cl)_2 \rightarrow Cu^{2+} + 2Cl^-$	$Cu(NO_3)_2 \rightarrow Cu^{2+} + 2NO_3^-$
$Zn(Cl)_2 \rightarrow Zn^{2+} + 2Cl^-$	$Zn(NO_3)_2 \rightarrow Zn^{2+} + 2NO_3^-$
$SnCl_2 \rightarrow Sn^{2+} + 2Cl^-$	$SnCl_2 \rightarrow Sn^{2+} + 2Cl^-$
$(NH_2)_2CS \rightarrow NH_2\text{-}C^+{=}NH + H^+ + S^{2-}$	$(NH_2)_2CS \rightarrow NH_2\text{-}C^+{=}NH + H^+ + S^{2-}$
$2Cu^{2+} + Zn^{2+} + Sn^{2+} + 4S^{2-} \rightarrow Cu_2ZnSnS_4$	$2Cu^{2+} + Zn^{2+} + Sn^{2+} + 4S^{2-} \rightarrow Cu_2ZnSnS_4$
$2Cu(Cl)_2{\cdot}2H_2O + Zn(Cl)_2 + SnCl_2{\cdot}2H_2O + 4(NH_2)_2CS + 8\,H_2O \rightarrow Cu_2ZnSnS_4 + 8NH_4Cl + 4CO_2$	$2Cu(NO_3)_2{\cdot}5H_2O + Zn(NO_3)_2{\cdot}6H_2O + SnCl_2{\cdot}2H_2O + 4CH_4N_2S \rightarrow Cu_2ZnSnS_4 + 6NH_4NO_3 + 2NH_4Cl + 4CO_2 + 5H_2O$

nature of the both chloride and nitrate sols is acidic and the pH values of the sol used for spin coating thin films are ~0.3 and 0.1 for chloride and nitrate sols, respectively.

The 2.5 cm × 2.5 cm glass substrates are cleaned using a soap solution followed by ultrasonic rinsing in acetone and de-ionized (DI) water for 10 min. These cleaned substrates are used for CZTS thin film fabrication using both chloride and nitrate based sols. The sols are spin coating at 2600 rpm and dried at 250 °C over a hot plate in the open air conditions. The spin coating and drying processes are repeated for three times to achieve the desired thickness, and thus, synthesized CZTS thin films are used for the characterization.

B. Characterization

The crystalline structure of film has been studied using X-ray diffractometer (Bruker D8 Advance) with a Cu K_α ($\lambda = 1.5406$ Å) monochromatic incident radiation source, operating at 40.0 kV and 40.0 mA. XRD data were collected in detector scan mode with incident X-ray source fixed at the 3° glazing incident angle and the detector has moved to collect the 2θ diffraction ranging from 20° to 80° at a step size of 0.02° per second. The room temperature Raman spectroscopy measurements are carried out using BaySpec. Inc. multi-wavelength spectrometer using 532 nm incident radiation. Scanning electron microscopy (SEM) measurements are carried out using EVO 18, especial edition, Carl Zeiss scanning electron microscopy (SEM) and the elemental compositions for these film structures are calculated by using an energy dispersive X-ray (EDX) (OXFORD instrument attached with SEM). The thicknesses of these films are characterized using Dektak XT stylus surface profiler (Bruker). Spectral diffuse reflectance has been measured using an 110 mm integrated sphere diffuse reflectance accessory integrated with a Carry 4000 UV-Vis spectrophotometer for these absorber structures in the 300–900 nm (UV-visible) wavelength range. A polytetrafluoroethylene (PTFE) sample was used as a reference for diffuse reflectance measurements. The current-voltage (I–V) and resistivity measurements are done using Keithley 4200 semiconductor characterization system (SCS) in two and four probe geometries, respectively.

III. RESULTS AND DISCUSSION

The CZTS films are subjected to heat treatment at different temperatures 250, 300, and 350 °C for half an hour over the hot plate under air ambiance for both chloride precursors (represented as MX thin films afterward) and nitrate precursors (represented as MXN thin films afterward). X-ray diffraction patterns on these structures are summarized in Fig. 2 for both MX and MXN thin films annealed at different temperatures.

The diffraction peaks at $2\theta \sim 28.4^0$, 47.5^0, and 56.3^0 are matched with the standard ICDD # 0260575 kesterite CZTS reference and correspond to (112), (220), and (312) crystal planes, respectively, also marked in Fig. 2 for easy identification. These measurements confirm the formation of CZTS kesterite crystallographic phase. These XRD measurements suggest that CZTS

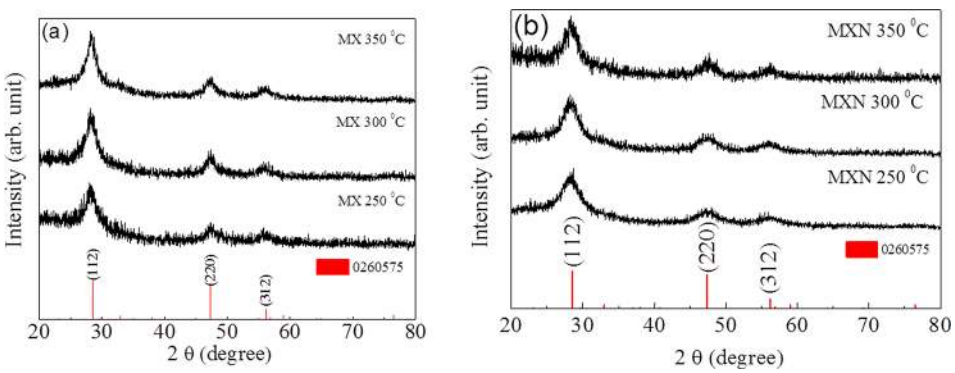

FIG. 2. XRD graphs for CZTS thin films at different annealing temperatures: (a) Chloride precursor route (MX) and (b) nitrate precursor route (MXN) derived thin films.

films are relatively textured along (1 1 2) axis and the crystallinity of these films enhanced with an increase in the annealing temperature, as shown in Fig. 2. The texture coefficient (TC (h k l)) has been calculated using $TC(h\,k\,l) = \frac{\frac{I(hkl)}{I_0(hkl)}}{N^{-1}\sum\frac{I(hkl)}{I_0(hkl)}}$; where N is the order of reflection, I is the measured intensity, and I_0 is the standard intensity taken from International Crystallographic Diffraction Data (ICDD) # 026-0575 as a reference.[28] The grain size (D) of the prepared thin film is calculated using Scherrer's formula: $Grain\,size = \frac{0.94*\lambda}{B\cos\theta}$, where B is full width half maxima (FWHM) of the diffraction peak measured in radians, λ is the wavelength of characteristic Cu K_α X-ray incident radiation.[28] The dislocation density (δ), which is length of dislocation lines per unit volume, is calculated using Williamsons and Smallman's equation $\delta = \frac{n}{D^2}$, where n is equal to unity for minimum dislocation density and D is the crystallite size.[29] The measured (112) textured crystallinity is summarized in Fig. 3(a) for different temperature annealed MX and MXN CZTS film structures, synthesized using chloride and nitrate sols, respectively. The (112) textured crystallinity for MX CZTS films prepared using chloride sol is relatively greater than that of nitrate routes prepared MXN CZTS films, suggesting chloride sol route may lead to relatively better textured film structures as compared to nitrate sol routes.

The measured grain size and dislocation density as a function of annealing temperature are plotted in Fig. 3(b) for these CZTS thin films structures. These measurements suggest that grain size has increased after annealing at higher temperatures for both chloride and nitrate sols prepared CZTS thin films. However, the grain size is always larger for chloride sol derived MX CZTS thin films as compared to that of the nitrate sol derived MXN CZTS thin film structures. The dislocation density has shown the inverse effect to that observed for grain size and has decreased with increase in annealing temperatures. Thus, these observations suggest that the higher annealing temperature may be a better choice for enhanced crystallographic and microstructural properties. However, annealing at higher temperatures (>350 °C) in an open ambient has shown adverse effects on crystallinity and phase purity, leading to the formation of oxides, secondary and ternary sulfide impurity phases. In addition, CZTS thin films showed enhanced sulfur and zinc loss and elemental oxide formation has also been observed for heating beyond 350 °C annealing temperatures.

The strain in these films has been estimated using $\varepsilon = \frac{B\cos\theta}{4}$ relation[30] and measured strains are summarized in Table II. The stacking fault probability, α, is the probability for the layers undergoing stacking fault in the film, defined as $\alpha = \left[\frac{2\pi^2}{45\sqrt{3}\tan\theta}\right]\Delta(2\theta)$; where θ is the measured (1 1 2) Bragg's angle.[31] The values of stacking fault probabilities are calculated using the measured (1 1 2) peak shift with reference to the ICDD database No. 026-05752 ($\Delta 2(\theta)$) and values are listed in Table II. This stacking fault probability suggests that one fault is likely to found in $1/\alpha$ layer. The presence of stacking fault gives rise to shift in peak positions corresponding to different reflection planes. The calculated stacking fault probability suggests that the stacking faults are decreasing with the increase in the annealing temperature. [This is the reason for

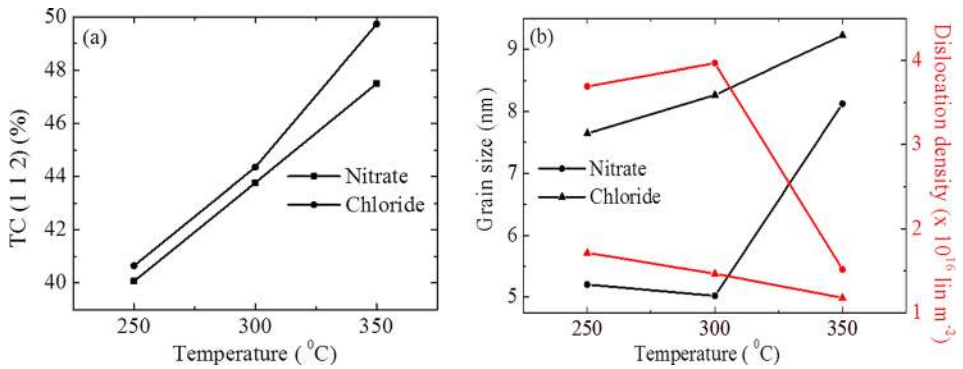

FIG. 3. (a) Texture coefficient and (b) Grain size and dislocation density variation as a function of the annealing temperature for MX and MXN CZTS thin films.

TABLE II. 2θ value for (1 1 2) crystallographic plane, FWHM, average crystallite size, dislocation density, strain, stacking fault probability for CZTS thin film prepared with different routes and different annealing conditions.

Sample	Temperature	2θ for (1 1 2) plane	FWHM	Average crystallite size (nm)	Dislocation density ($\delta \times 10^{16}$) (line m^{-2})	Strain (ε) (line^{-2} m^{-4})	Stacking fault probability (α)
MX	250	28.234	1.72	7.64	1.71	0.417	0.299
	300	28.344	1.70	8.27	1.46	0.411	0.187
	350	28.357	0.88	9.22	1.17	0.213	0.174
MXN	250	28.279	1.66	5.20	3.69	0.402	0.253
	300	28.296	2.08	5.02	3.96	0.504	0.236
	350	28.406	1.40	8.13	1.51	0.337	0.125

observed shift in the diffraction peaks of low temperature annealed thin films, which approached to the correct 2θ value for high temperature annealed CZTS thin films.]

The room temperature Raman measurements are carried out on 300 °C CZTS thin films and results are summarized in Fig. 4 The observed intense peak at ~331 cm^{-1} and two small vibrational peaks at ~169 and 252 cm^{-1} correspond to the characteristic Raman modes for kesterite CZTS phase, substantiating the X-ray diffraction measurements and are also in agreement with the previously reported data.[32] The strongest vibrational mode at 331 cm^{-1} has been attributed to the local structural inhomogeneity within the disordered cation sublattice and suggests the Cu-poor CZTS material. The recorded spectrum do not exhibit any vibration modes corresponding to impurity/secondary phases such as CuS (474 cm^{-1}),Cu_2S (472 cm^{-1});[33] ZnS(278, 351 cm^{-1});[34] SnS(192 cm^{-1});[35] and SnS_2 (205, 315 cm^{-1})[36] binary secondary phases and Cu_2SnS_3 (CTS) (303, 355 cm^{-1} for cubic CTS and 336, 351 cm^{-1} for tetragonal CTS) ternary secondary phases.[37,38] The absence of any of these vibrational modes substantiates the crystallographic kesterite phase purity even at the microscopic level. The results suggest the formation of kesterite phase growth with Cu-deficient CZTS thin films is in agreement with the EDX results, discussed later.

The microstructural properties and elemental distributions are investigated using scanning electron microscopy (SEM) and energy dispersive X-ray (EDX) measurements. The microscopic results are summarized in Fig. 5 for both chloride and nitrate sols derived CZTS thin film structures annealed at 300 °C temperature. SEM micrographs suggest that CZTS films synthesized using chloride sol are highly uniform across the entire film, Fig. 5(a), with respect to

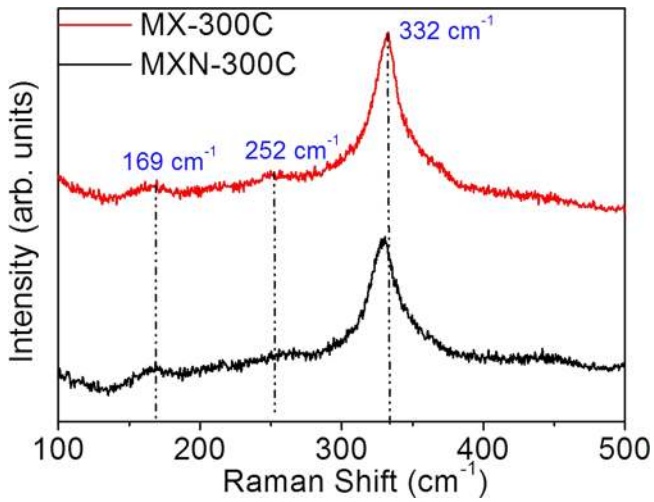

FIG. 4. Raman spectroscopy measurement of 300 °C annealed MX and MXN CZTS thin films.

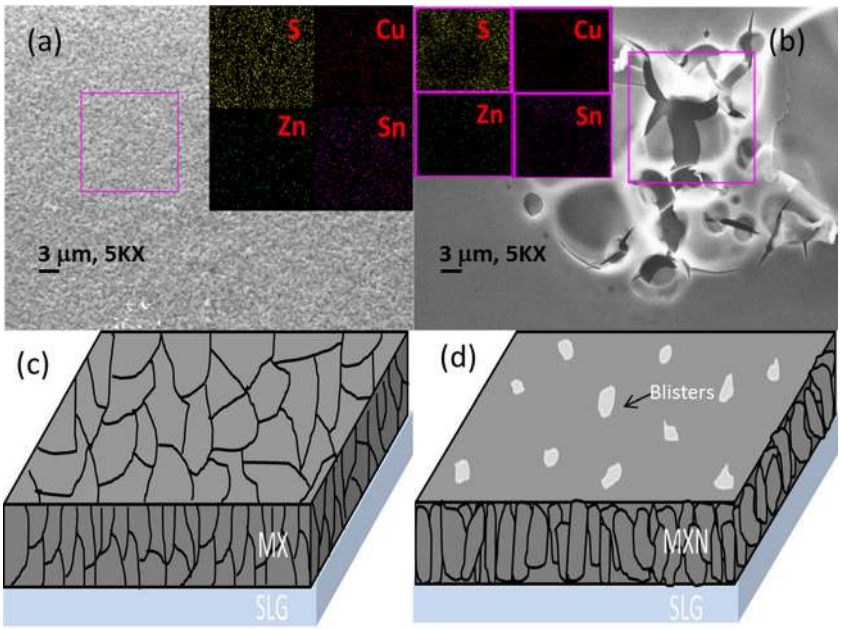

FIG. 5. (a) SEM micrograph and EDX mapping (inset) for chloride precursor film (b) SEM micrograph and EDX mapping (inset) for nitrate precursor film andan schematic 3D view of (c) chloride precursor derived film, showing polycrystalline film with large grains; (d) nitrate precursor film, showing large blisters at the surface.

the nitrate sol derived thin films, which consists of large cracks and voids, as shown in Fig. 5(b). The observed larger grains for chloride sol derived CZTS thin film substantiate the XRD results, as discussed earlier. The surface of CZTS films gets denser with increasing the annealing temperature for chloride sol derived films. The surface texture schematics are represented in Figs. 5(c) and 5(d), showing the observed large and dense grain morphology for chloride precursor derive MX CZTS films and non-uniform growth with voids and cracks surface morphology for nitrate precursor derived MXN CZTS films. The voids and cracks in MXN CZTS thin films may provide possible shunt paths during device fabrication and may result in poor electrical performance, consistent with observed electrical properties for these films, as discussed later. The elemental compositions on these CZTS film structures have been evaluated in several areas across the films and also elemental mapping has been carried out to understand the distribution of different elements across the film. The elemental mapping shows a uniform distribution of constituent elements in chloride sol derived CZTS thin films, as shown in the inset of Fig. 5(a). There are cracks and defects due to blistering effect, observed in nitrate sol derived MXN CZTS films, which are visible even at lower magnifications, Fig. 5(b). These MXN CZTS films are also not well adhered to the substrate surface. The possible reason may be the observed compressive stress in the film or due to the micro-bubbles of trapped gasses during synthesis into the material, which blistered at the time of thermal treatment, consistent with some of the earlier observations.[39] These films also consist of smooth regions, which are relatively defect free with small grains, as observed in XRD spectrums with relatively smaller intensity and wider full width at half maxima. The EDX mapping suggests that defective regions are deficient in copper, and tin, as shown in the inset of Fig. 5(b). In such defective regions, zinc composition is relatively uniform, suggesting the possibility for zinc to be at lower surfaces and the loss in tin and copper elements is attributed due to their relatively low vapor pressures. However, film composition is relatively uniform across such smooth areas.

The detailed elemental composition variation as a function of annealing temperatures for these CZTS thin films is summarized in Fig. 6. All CZTS structures treated at different temperatures, exhibit copper poor and slightly tin rich configurations. This is also in agreement with the observed EDX mapping at defective regions in nitrate precursor film which also showed

relatively uniform zinc concentration deep regions of these CZTS films. The cross-sectional SEM micrographs for both MX and MXN CZTS thin films annealed at 300 °C are shown in Figs. 7(a) and 7(c), in conjunction with tilted suface morphology with substrate surface, Figs. 7(b) and 7(d). These measurements confirm the formation of large, dense grains for chloride sol thin films throughout the film surface, whereas despite relatively dense structures, large cracks are propagated from the surface down to the interface for nitrate sol thin films, as marked in Figs. 7(c) and 7(d), indicated with blistered regions. This is consistent with the observed surface blisters, as shown in Fig. 5(b) for nitrate sol thin films, discussed earlier. These cross-sectional micrographs with tilted film structures also confirm that the chloride sol thin films are highly uniform, less defective in conjunction with the dense surface morphology as compared to that of nitrate sol thin films.

The diffuse reflectance measurements are collected in the 300–900 nm wavelength range and the measurements are used to calculate the spectral absorptance, using the Kubelka-Munk model $F(R) = \frac{(100-R)^2}{2R}$, where F(R) is the Kubelka-Munk function and R is the percent diffuse reflectance. The calculated F(R) has been used to understand the optical bandgap of these CZTS thin film structures using the Tauc relation $(\alpha h\nu)^{\frac{1}{n}} = A(h\nu - Eg)$, where α is the absorption coefficient, h is Plank's constant, ν is the photon frequency, A is the proportionality constant, and E_g is the bandgap of the material.[40] The exponent n signifies the nature of optical bandgap transition. The exponent n can take 1/2, 3/2, 2, and 3 values corresponding to direct allowed, direct forbidden, indirect allowed, and indirect forbidden transitions, respectively. In the present case, $(F(R)h\nu)^2$ versus energy $h\nu$ exhibit the correct absorption trend (as α is proportional to F(R)) and thus used to calculate the optical bandgap using these plots, as shown in Fig. 8. The intercept of extrapolated linear region in these plots on energy axis represents the optical bandgap and direct bandgap of these CZTS films is ~1.52 eV for both chloride and nitrate sols derived CZTS thin films.

These measurements, Fig. 8(a), suggest that the annealing temperature has no significant effect on the optical bandgap for chloride sol derived CZTS thin films. However, a small decrease in the optical bandgap has been observed for nitrate sol derived CZTS film structures. The most important observation is that the absorption is an order of magnitude smaller in the case of nitrate sol derived CZTS thin films and reduced drastically for high temperature annealed thin films. This is not the case for chloride sol derived CZTS thin films, and absorption is nearly independent of temperature. The observed poor absorption in nitrate sol derived CZTS thin films is consistent with observed large defect density from both XRD and SEM measurements. Refractive index and dielectric constant are calculated using modified Moss relation $E_g n^4 = 108$ eV.[41] The static dielectric constant ($\varepsilon_{\text{static}}$) and high frequency dielectric constant (ε_∞) are calculated using the relations $\varepsilon_{static} = 18.52 - 3.08\,E_g$ and $\varepsilon_\infty = n^2$.[31] The calculated values of n, $\varepsilon_{\text{static}}$, ε_∞ for CZTS thin film corresponding to bandgap value of 1.52 eV are 2.9033, 13.8384, and 8.4292, respectively, consistent with the reported literature values.[31]

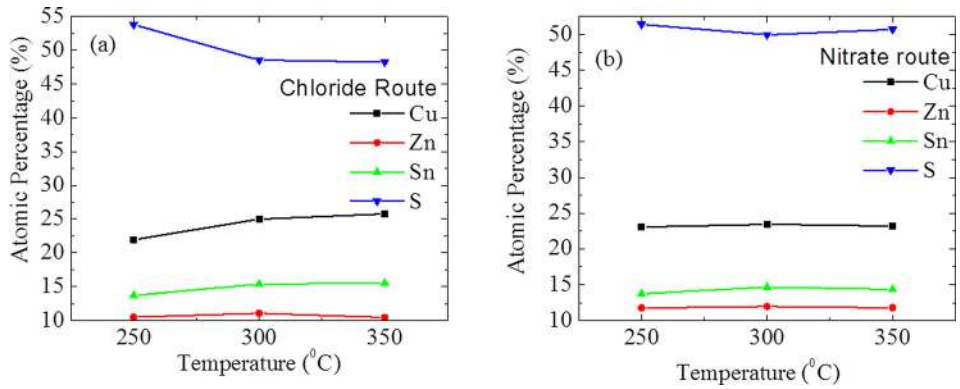

FIG. 6. EDX compositional plot for films processed at different annealing temperature for (a) chloride route and (b) nitrate route.

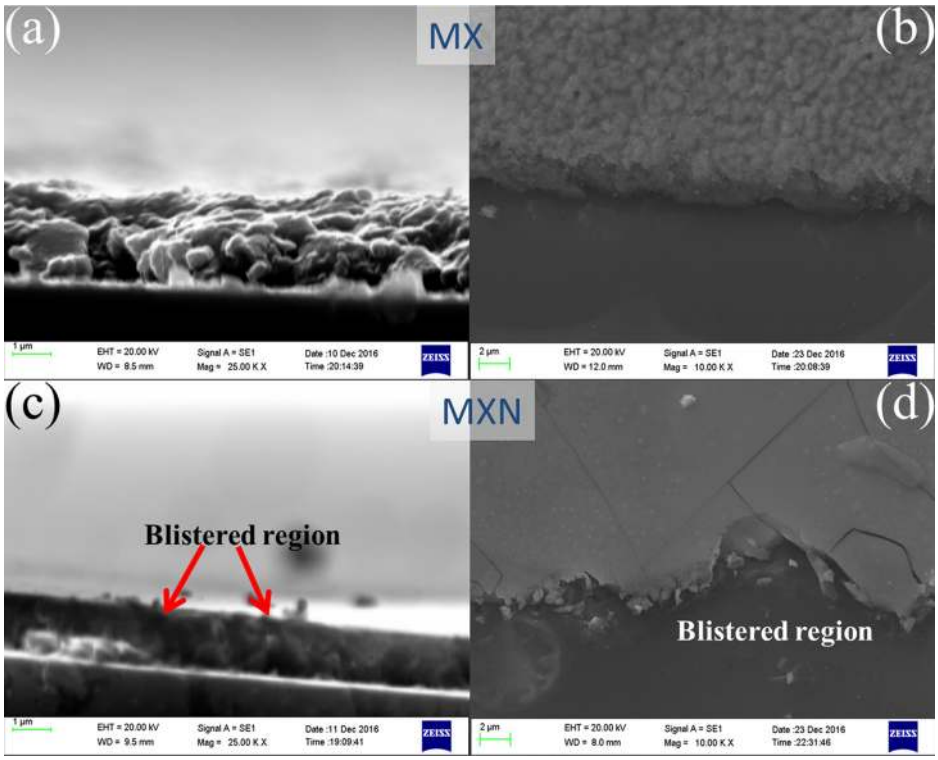

FIG. 7. Cross-sectional SEM micrographs for 300 °C annealed (a) chloride route (MX) (c) nitrate route derived (MXN) CZTS thin films and corresponding surface morphology of (b) chloride route (MX) and (d) nitrate route derived (MXN) CZTS thin films.

Resistivity measurements are carried out in four point van der Pauw configuration, and resistivity mapping is done by taking a measurement at different places across $1' \times 1'$ CZTS thin films. For resistivity mapping, the 300 °C annealed sample has been chosen since this temperature has resulted in desired CZTS thin film structures with respect to other CZTS samples treated at different temperatures. The measured resistivities across the CZTS thin films are plotted in Fig. 9 and suggesting that chloride sol based CZTS thin film structures exhibit uniform resistivity distribution as compared to that nitrate sol derived CZTS thin film structures.

It can be seen from the resistivity mapping that chloride precursor film shows very low resistivity values with smaller variation $0.025 \pm 0.008\ \Omega\,\text{cm}$ across the entire thin film. This confirms that chloride precursor shows uniform film growth. However, nitrate precursor film shows large resistivity values and the variation in resistivity is very high $31.70 \pm 26.2\ \Omega\,\text{cm}$

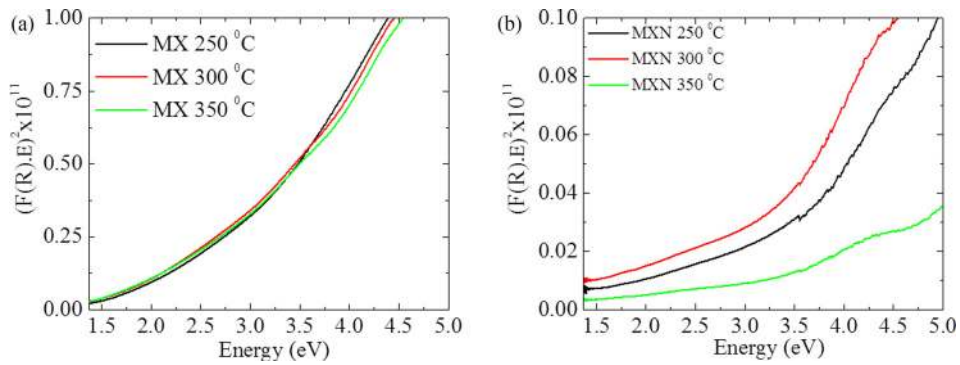

FIG. 8. $(\alpha \cdot E)^2$ vs. photon energy plot for films processed at different baking temperature for (a) chloride precursor route and (b) nitrate precursor route.

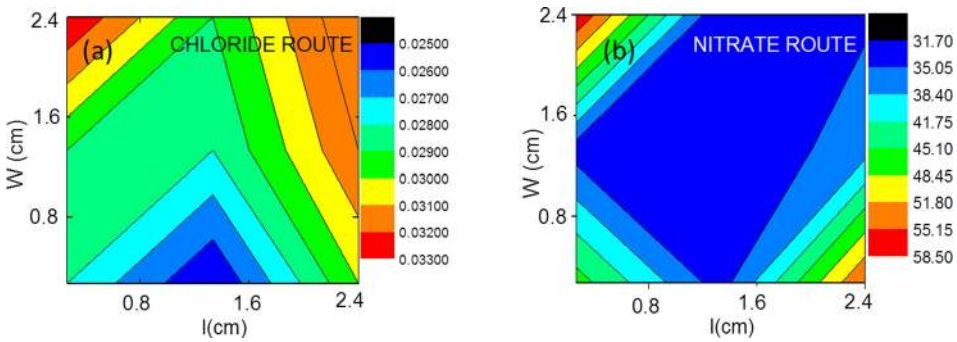

FIG. 9. van der Paw resistivity mapping of sample prepared at temperature 300 °C on 1 in. × 1 in. CZTS/glass at different positions using (a) chloride precursor route and (b) nitrate precursor route.

which confirms that film is not uniform and defects are present in the sample, as confirmed by XRD and microscopic measurements.

Further, current-voltage (I–V) characteristics of these CZTS thin films are carried out using two point contact method. The I–V characteristics are plotted in Fig. 10 and suggest that chloride sol derived CZTS films are less resistive as compared to that of nitrate sol derived CZTS thin films. The conductivity further increases with annealing temperatures. The insets in Figs. 10(a) and 10(b) show the effect of temperature on resistivity value for chloride and nitrate precursor films, respectively. The possible reason for this increased conductivity of the CZTS film is its increased grain size and lesser defects at higher temperature. Nitrate sol derived CZTS thin films show very poor conductivity compared to that of chloride sol derived CZTS films. The less conductivity for nitrate derived CZTS films is mainly attributed to the presence of cracks and defects, which do not allow a continuous path for the electrical current flow. The thickness of the nitrate precursor films is only 0.8 μm compared to chloride precursor films, which are ~1.8 μm thick. This may also contribute to its higher re sistivity value. The increasing resistivity of MXN CZTS films with annealing temperature may be attributed to the increased defects and dislocations, leading to the discontinuity across the film despite the observed larger grains size.

The space charge limited current conduction is defined as $I = \frac{9}{8}\,\varepsilon_r\varepsilon_0\theta\mu\frac{V^n}{d^3}$, where V is the applied field, d is the distance across the electrode, ε_0 is the permittivity of free space, ε_r is dielectric constant of material, θ is the ratio of free electrons to the trapped electrons, and n is the power factor.[42] Assuming single discrete shallow trap level in the prepared films, the trapped electron density, N_t, can be calculated from trap filled limit voltage (V_{TFL}) using $N_t = \frac{9}{8q}\,\varepsilon_r\varepsilon_0\frac{V_{TFL}}{d^2}$; where q is the charge and physical meaning of other symbols is same as explained above. The logarithm of current and field plots is derived from the measured current–voltage characteristics and is

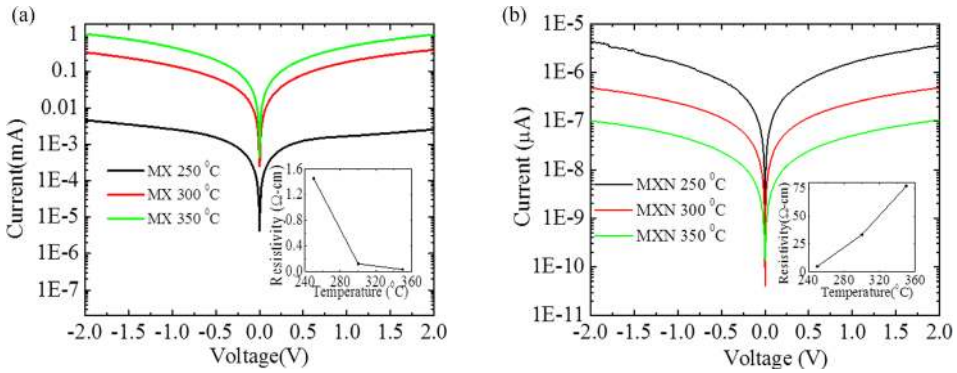

FIG. 10. Current-voltage characteristics of films prepared using (a) chloride precursor route and (b) nitrate precursor route. Inset in both the graph represents resistivity measured using van der Paw configuration for the respective films.

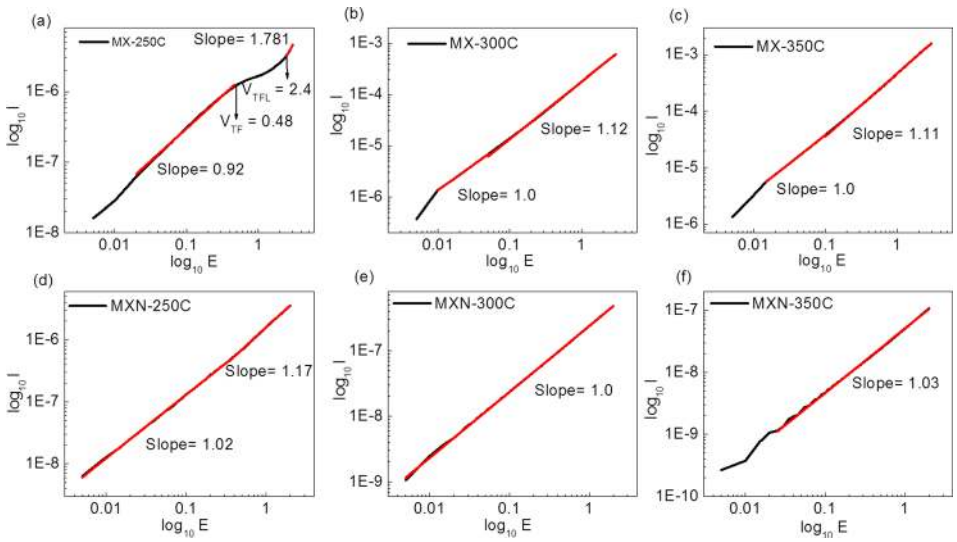

FIG. 11. Logarithmic current versus applied field plots for CZTS thin film prepared ((a)–(c)) using chloride precursor route (MX) and ((d)–(f)) using nitrate precursor route (MXN).

summarized in Fig. 11. These measurements suggest that current conduction is ohmic for both MX and MXN CZTS thin films as the slope of these curves is nearly unity, as shown in Fig. 11. However, the low temperature ~250 °C annealed MX CZTS thin films have shown ohmic electrical conduction behavior at lower applied field up to 0.34 V/cm and space charge assisted current conduction (slope is ~1.8) for higher applied fields, as shown in Fig. 9(a). The estimated trap filled limited voltage (V_{TFL}) is ~2.4 V/cm, which corresponds to the trapped electron density $\sim 2.07 \times 10^{9}\,cm^{-3}$ in this MX CZTS thin film structure. In addition, the slope has started deviating from unity at or above 0.48 V/cm applied field, suggesting the deviation from the normal ohmic behavior. This behavior has not been observed in higher temperature annealed and also for MXN CZTS thin film structures.

IV. CONCLUSION

Two different metal salt precursors derived routes have been investigated for preparing a suitable sol to synthesize the spin coated CZTS thin film as an absorber for solar photovoltaic applications. The observed results suggest that the nearly stoichiometric uniform thin film structures can be prepared using chloride sol without any additional sulfurization at higher temperatures. The chloride sol derived CZTS thin films annealed at 300 °C exhibits good structural, optical, and electrical responses as compared to that of nitrate sol derived CZTS thin films. The uniform resistivity distribution and enhanced electrical response have been achieved for MX CZTS thin films under controlled sol conditions and optimized annealing temperatures, suggesting it as a suitable choice for heterostructure solar cell devices. The optimized synthesis can be scaled for larger area deposition for photovoltaic applications. In contrast, the nitrate sol derived CZTS films are not suitable due to the large intrinsic cracks and voids appeared because of blistering effects during synthesis and post-synthesis treatment. These voids and cracks provide the active sites for etching of the bottom molybdenum back contact during cadmium sulfide "CdS" buffer layer deposition on CZTS thin films and thus hampering the device fabrication and its performance.

ACKNOWLEDGMENTS

The author Ambesh Dixit acknowledges the Department of Science and Technology (DST), Government of India, through Grant No. DST/INR/ISR/P-12/2014 for carrying out this experimental work.

[1]P. Jackson, D. Hariskos, R. Wuerz, O. Kiowski, A. Bauer, T. M. Friedlmeier, and M. Powalla, "Properties of Cu(In,Ga)Se_2 solar cells with new record efficiencies up to 21.7%," Phys. Status Solidi RRL **9**, 28–31 (2015).
[2]M. A. Green, K. Emery, Y. Hishikawa, W. Warta, and E. D. Dunlop, "Solar cell efficiency tables (version 48)," Prog. Photovoltaics: Res. Appl. **24**, 905–913 (2016).
[3]X. Xin, M. He, W. Han, J. Jung, and Z. Lin, "Low-cost copper zinc tin sulfide counter electrodes for high-efficiency dye-sensitized solar cells," Angew. Chem. Int. Ed. **50**, 11739–11742 (2011).
[4]P. Dai, G. Zhang, Y. Chen, H. Jiang, Z. Feng, Z. Lin, and J. Zhan, "Porous copper zinc tin sulfide thin film as photocathode for double junction photoelectrochemical solar cells," Chem. Commun. **48**, 3006 (2012).
[5]K. V. Gurav, S. W. Shin, U. M. Patil, P. R. Deshmukh, M. P. Suryawanshi, G. L. Agawane, S. M. Pawar, P. S. Patil, J. Y. Lee, C. D. Lokhande, and J. H. Kim, "Cu_2ZnSnS_4 (CZTS)-based room temperature liquefied petroleum gas (LPG) sensor," Sens. Actuators, B **190**, 408–413 (2014).
[6]N. M. Shinde, P. R. Deshmukh, S. V. Patil, and C. D. Lokhande, "Development of polyaniline/Cu_2ZnSnS_4 (CZTS) thin film based heterostructure as room temperature LPG sensor," Sens. Actuators. A **193**, 79–86 (2013).
[7]X. Yu, X. An, A. Genç, M. Ibáñez, J. Arbiol, Y. Zhang, and A. Cabot, "Cu_2ZnSnS_4–PtM (M = Co, Ni) nanoheterostructures for photocatalytic hydrogen evolution," J. Phys. Chem. C. **119**, 21882–21888 (2015).
[8]J. Wang, P. Zhang, X. Song, and L. Gao, "Surfactant-free hydrothermal synthesis of $Cu_2ZnSnS4$ (CZTS) nanocrystals with photocatalytic properties," RSC Adv. **4**, 27805 (2014).
[9]F. Jiang, Gunawan, T. Harada, Y. Kuang, T. Minegishi, K. Domen, and S. Ikeda, "Pt/In_2S_3/CdS/Cu_2ZnSnS_4 thin film as an efficient and stable photocathode for water reduction under sunlight radiation," J. Am. Chem. Soc. **137**, 13691–13697 (2015).
[10]M. Johnson, S. V. Baryshev, E. Thimsen, M. Manno, X. Zhang, I. V. Veryovkin, C. Leighton, and E. S. Aydil, "Alkali-metal-enhanced grain growth in Cu_2ZnSnS_4 thin films," Energy Environ. Sci. **7**, 1931–1938 (2014).
[11]A. Nagaoka, H. Miyake, T. Taniyama, K. Kakimoto, Y. Nose, M. A. Scarpulla, and K. Yoshino, "Effects of sodium on electrical properties in Cu_2ZnSnS_4 single crystal," Appl. Phys. Lett. **104**, 152101 (2014).
[12]B. P. Rand, J. Genoe, P. Heremans, and J. Poortmans, "Solar cells utilizing small molecular weight organic semiconductors," Prog. Photovoltaics: Res. Appl. **15**, 659–676 (2007).
[13]S.-N. Park, S.-J. Sung, J.-H. Sim, K.-J. Yang, D.-K. Hwang, J. Kim, G. Y. Kim, W. Jo, D.-H. Kim, and J.-K. Kang, "Nanostructured p-type CZTS thin films prepared by a facile solution process for 3D p-n junction solar cells," Nanoscale **7**, 11182–11189 (2015).
[14]J. Kong, Z.-J. Zhou, M. Li, W.-H. Zhou, S.-J. Yuan, R.-Y. Yao, Y. Zhao, and S.-X. Wu, "Wurtzite copper-zinc-tin sulfide as a superior counter electrode material for dye-sensitized solar cells," Nanoscale Res. Lett. **8**, 464 (2013).
[15]T. P. Dhakal, C. Y. Peng, R. Reid Tobias, R. Dasharathy, and C. R. Westgate, "Characterization of a CZTS thin film solar cell grown by sputtering method," Sol. Energy **100**, 23–30 (2014).
[16]T. Kubart, T. Ericson, J. J. Scragg, M. Edoff, and C. Platzer-Björkman, "Reactive sputtering of Cu_2ZnSnS_4 thin films—Target effects on the deposition process stability," Surf. Coat. Technol. **240**, 281–285 (2014).
[17]T. Ericson, T. Kubart, J. J. Scragg, and C. Platzer-Björkman, Thin Solid Films **520**, 7093–7099 (2012).
[18]B. Shin, O. Gunawan, Y. Zhu, N. A. Bojarczuk, S. J. Chey, and S. Guha, "Thin film solar cell with 8.4% power conversion efficiency using an earth-abundant Cu_2ZnSnS_4 absorber," Prog. Photovoltaics **21**, 72–76 (2013).
[19]J. Wang, P. Zhang, X. Song, and L. Gao, "Cu_2ZnSnS_4 thin films: Spin coating synthesis and photoelectrochemistry," RSC Adv. **4**, 21318 (2014).
[20]K. D. Zhang, Z. R. Tian, J. B. Wang, B. Li, X. L. Zhong, D. Y. Guo, and S. M. He, "Preparation of Cu_2ZnSnS_4 thin films using spin-coating method with thermolysis and annealing," J. Sol-Gel Sci. Technol. **73**, 452–459 (2015).
[21]K. Tanaka, N. Moritake, and H. Uchiki, "Preparation of Cu_2ZnSnS_4 thin films by sulfurizing sol–gel deposited precursors," Sol. Energy Mater. Sol. Cells **91**, 1199–1201 (2007).
[22]K. Tanaka, Y. Fukui, N. Moritake, and H. Uchiki, "Chemical composition dependence of morphological and optical properties of Cu_2ZnSnS_4 thin films deposited by sol–gel sulfurization and Cu_2ZnSnS_4 thin film solar cell efficiency," Sol. Energy Mater. Sol. Cells **95**, 838–842 (2011).
[23]K. Tanaka, M. Oonuki, N. Moritake, and H. Uchiki, "Cu_2ZnSnS_4 thin film solar cells prepared by non-vacuum processing," Sol. Energy Mater. Sol. Cells **93**, 583–587 (2009).
[24]J. A. Bwamba, N. Alu, K. K. Adama, Z. Abdullahi, U. U. Iwok, A. C. Egba, and A. A. Oberafo, "Characterization of CZTS absorbent material prepared by field-assisted spray pyrolysis," Am. J. Mater. Sci. **4**, 127–132 (2014).
[25]S. S. Mali, P. S. Shinde, C. A. Betty, P. N. Bhosale, Y. W. Oh, and P. S. Patil, "Synthesis and characterization of Cu_2ZnSnS_4 thin films by SILAR method," J. Phys. Chem. Solids **73**, 735–740 (2012).
[26]M. P. Suryawanshi, S. W. Shin, U. V. Ghorpade, K. V. Gurav, C. W. Hong, and A. V. Moholkar, "Improved photoelectrochemical performance of Cu_2ZnSnS_4 (CZTS) thin films prepared using modified successive ionic layer adsorption and reaction (SILAR) sequence," Electrochim. Acta **150**, 136–145 (2014).
[27]S. Chen, H. Tao, Y. Shen, L. Zhu, X. Zeng, J. Tao, and T. Wang, "RSC advances treatment," RSC Adv. **5**, 6682–6686 (2015).
[28]V. Bilgin, S. Kose, F. Atay, and I. Akyuz, "The effect of substrate temperature on the structural and some physical properties of ultrasonically sprayed CdS films," Mater. Chem. Phys. **94**, 103–108 (2005).
[29]G. K. Williamson and R. E. Smallman, "III. Dislocation densities in some annealed and cold-worked metals from measurements on the X-ray debye-scherrer spectrum," Philos. Mag. **1**, 34–46 (1956).
[30]M. Y. Ali, "The effect of copper concentration on structural, optical and dielectric properties of $Cu_xZn_{1-x}S$ thin films," Opt. Commun. **285**, 1215–1220 (2012).
[31]J. Henry, K. Mohanraj, and G. Sivakumar, "Electrical and optical properties of CZTS thin films prepared by SILAR method," J. Asian Ceram. Soc. **4**, 81–84 (2016).
[32]P. R. Ghediya and T. K. Chaudhuri, "Dark and photo-conductivity of doctor-bladed CZTS films above room temperature," J. Phys. D: Appl. Phys. **48**, 455109 (2015).
[33]B. Minceva-Sukarova, M. Najdoski, I. Grozdanov, and C. J. Chunnilall, "Raman spectra of thin solid films of some metal sulfides," J. Mol. Struct. **410–411**, 267–270 (1997).
[34]Y. C. Cheng, C. Q. Jin, F. Gao, X. L. Wu, W. Zhong, S. H. Li, and P. K. Chu, "Raman scattering study of zinc blende and wurtzite ZnS," J. Appl. Phys. **106**, 123505 (2009).

[35]H. R. Chandrasekhar, R. G. Humphreys, U. Zwick, and M. Cardona, "Infrared and Raman spectra of the IV–VI compounds SnS and SnSe," Phys. Rev. B **15**, 2177–2183 (1977).
[36]A. J. Smith, P. E. Meek, and W. Y. Liang, "Raman scattering studies of SnS_2 and $SnSe_2$," J. Phys. C: Solid State Phys. **10**, 1321–1333 (1977).
[37]P. A. Fernandes, P. M. P. Salomé, and A. F. da Cunha, "A study of ternary Cu_2SnS_3 and Cu_3SnS_4 thin films prepared by sulfurizing stacked metal precursors," J. Phys. D: Appl. Phys. **43**, 215403 (2010).
[38]P. A. Fernandes, P. M. P. Salomé, and A. F. Da Cunha, "Cu_xSnS_{x+1} ($x = 2, 3$) thin films grown by sulfurization of metallic precursors deposited by dc magnetron sputtering," Phys. Status Solidi **7**, 901–904 (2010).
[39]C. Malerba, M. Valentini, C. L. Azanza Ricardo, A. Rinaldi, E. Cappelletto, P. Scardi, and A. Mittiga, "Blistering in Cu_2ZnSnS_4 thin films: Correlation with residual stresses," Mater. Des. **108**, 725 (2016).
[40]J. Tauc, R. Grigorovici, and A. Vancu, "Optical properties and eletronic structure of amorphous germanium," Phys. Status Solidi **15**, 627–637 (1966).
[41]P. Gupta and R. Ravindra, "Comments on the Moss formula," Phys. Status Solidi B **100**, 715–719 (1980).
[42]B. Ramachandran, A. Dixit, R. Naik, G. Lawes, and M. S. R. Rao, "Charge transfer and electronic transitions in polycrystalline $BiFeO_3$," Phys. Rev. B **82**, 012102 (2010).